Heliyon 9 (2023) e13705

Contents lists available at ScienceDirect

Heliyon

journal homepage: www.cell.com/heliyon

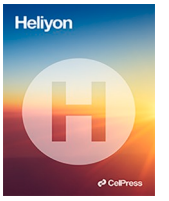

Research article

pH-responsive gelatin polymer-coated silica-based mesoporous composites for the sustained-release of indomethacin

Bo Yu [a,b,1], Ruiping Shi [a,1], Chunlai Liu [a], Zelong Liu [a], Peihang Shen [a], Jianglei Hu [a,*], Fengwei Shi [a,*]

[a] School of Chemical Engineering & Advanced Institute of Materials Science, Changchun University of Technology, Changchun 130012, China
[b] College of Pharmacy, Changchun University of Chinese Medicine, Changchun 130117, China

ARTICLE INFO

Keywords:
SBA-16
Mesoporous
Gelatin coating
Drug carrier
pH-responsive
In vitro release

ABSTRACT

This paper prepared drug-loaded mesoporous silica composites with a pH-responsive type. These composites were prepared by using three-dimensional caged silica (SBA-16) as the carrier, 3-aminopropyl trimethoxysilane (APTMS) as the silane coupling agent, and indomethacin (IMC) as the loaded drug, respectively. The drug-loaded precursor NH_2-SBA-16@IMC was prepared by solution diffusion adsorption. Finally, the pH-responsive drug-loaded composites NH_2-SBA-16@IMC@GA were synthesized by wrapping the NH_2-SBA-16@IMC with a condensation polymer of gelatin and glutaraldehyde. The composition and structure of the drug-loaded composites were characterized by FT-IR, XRD, TG, SEM, TEM, and N_2 adsorption-desorption. The in vitro simulated release performance of the drug-loaded composites was investigated at 37 °C under three pH conditions. The results show that the NH_2-SBA-16@IMC@GA can be released in response to specific pH environment, which can effectively control the release speed of the indomethacin.

1. Introduction

Nanotechnology in hygiene and medicine, namely nanomedicine, is one of the most promising and fascinating areas of research today [1, 2, 3, 4]. Nanoparticles are revolutionizing the medical field for disease treatment, physiology monitoring, and health protection. As drug carriers of nanomaterials, especially those capable of generating stimulatory responses, they can change the mechanism of drug metabolism and improve drug utilization. The carrier is administered in the case of the lesion, which can increase the efficacy of the drug and reduce the side effect of the drug. Therefore, it has been a greatly concerned for the scientific and technological, and industry [5, 6, 7, 8, 9, 10].

There are many types of drug carriers as nanomaterials, among which the research hotspots are mesoporous carbon and mesoporous silica, especially mesoporous silica is a material that has been hotly discussed in recent years. Since Mobil Corporation first reported the MCM-41 series of mesoporous silica molecular sieves, mesoporous silica materials have shown great application prospects [11]. Since then, mesoporous materials have attracted more and more attention as carriers for nano-drug systems and targeted therapy. In the past few decades, mesoporous silica materials have shown an increasing index of potential drug delivery applications, especially in oral dosage forms [12, 13, 14, 15, 16]. Szegedi et al. used different amounts of 3-aminopropyl triethoxysilane to prepare MCM-41

* Corresponding authors.
E-mail addresses: hujl863@163.com (J. Hu), sfw0403@163.com (F. Shi).
[1] B. Yu and R. Shi contributed equally to this work.

https://doi.org/10.1016/j.heliyon.2023.e13705
Received 3 December 2022; Received in revised form 2 February 2023; Accepted 8 February 2023
Available online 14 February 2023

with a spherical structure and small particle size (100 nm) for a comparative study of the adsorption and release of ibuprofen [17]. Xu's group reported that triethyl-modified MCM-41, only 75% of ibuprofen was released after 48 h, and pure silica MCM-41 was then released completely at 1 h. And with the increase of the grafting group, the release rate of ibuprofen also increases, so the control rate of ibuprofen release can be controlled by changing the grafting amount of trimethylsilane [18]. Although the drug-release performance of mesoporous molecules can be regulated by modifying the screening aperture and surface, it is still difficult to achieve real intelligent control of drug release. The more effective method is the high loading of mesoporous silica and other materials such as magnetic nanoparticles, and hydrogel, the stability of silica-based mesoporous materials, high loading, and intelligent materials responsiveness to the environment, build a new intelligent drug delivery system, which has become another research hotspot in recent years [19, 20, 21].

The pH-responsive type is the controlled release of drugs by modifying acid-degradable materials, pH-sensitive bonds, or polyelectrolytes on the surface of mesoporous silica. Han et al. prepared a pH-responsive multilayer nanocarrier material carrying doxorubicin and small interfering RNA (siR-NA). Under weak acid and neutral (phosphate buffer solution) conditions, doxorubicin and siRNA were hardly released within 24 h, while under acid conditions, they had obvious release behavior [22]. Shi's team using mesoporous hollow ball hollow core and interoporous shell through the pore and polyelectrolytes has the characteristics of environmental response, through layer upon layer self-assembly technology, wrapped in mesoporous hollow ball outer layer of polyelectrolyte to pH or ion strength conditions produce structural performance response, realize the mesoporous hole plugging and open, thus play a drug control release of "switch" role [23,24]. Cui et al. constructed a novel synthetic peptide brush-wrapped organic-inorganic nanohybrid drug delivery system (MSN@PBLGF), and achieved targeted and controlled release of the drug under GSH and thermal stimulation. The targeted and controlled release of the drug was achieved under GSH and thermal stimulation [25].

At present, there are many studies on the sustained release of two-dimensional hexagonal mesoporous silica as drug carriers, such as MCM-41 and SBA-15. Related studies based on three-dimensional cage-like structures have also been reported, such as SBA-16. Compared with the two-dimensional structure, the three-dimensional cubic cage structure has a larger cage diameter, but a smaller pore entrance and pore channel, which is more conducive to drug administration [26, 27, 28]. Therefore, it is more meaningful to use SBA-16 as a nano-drug carrier in this study [29, 30, 31, 32, 33, 34, 35, 36]. However, pH-responsive composites prepared with SBA-16 as the carrier, indoleomycin as the carrier center, and gel polymer as the coating agent have not been reported.

In this paper, the drug-loaded precursor NH_2-SBA-16@IMC was prepared by solution diffusion adsorption using SBA-16 as the carrier, APTMS as the silane coupling agent, and IMC as the drug-loaded center. Finally, the pH-responsive drug-loaded composites NH_2-SBA-16@IMC@GA were synthesized by wrapping the NH_2-SBA-16@IMC with a condensation polymer of gelatin with

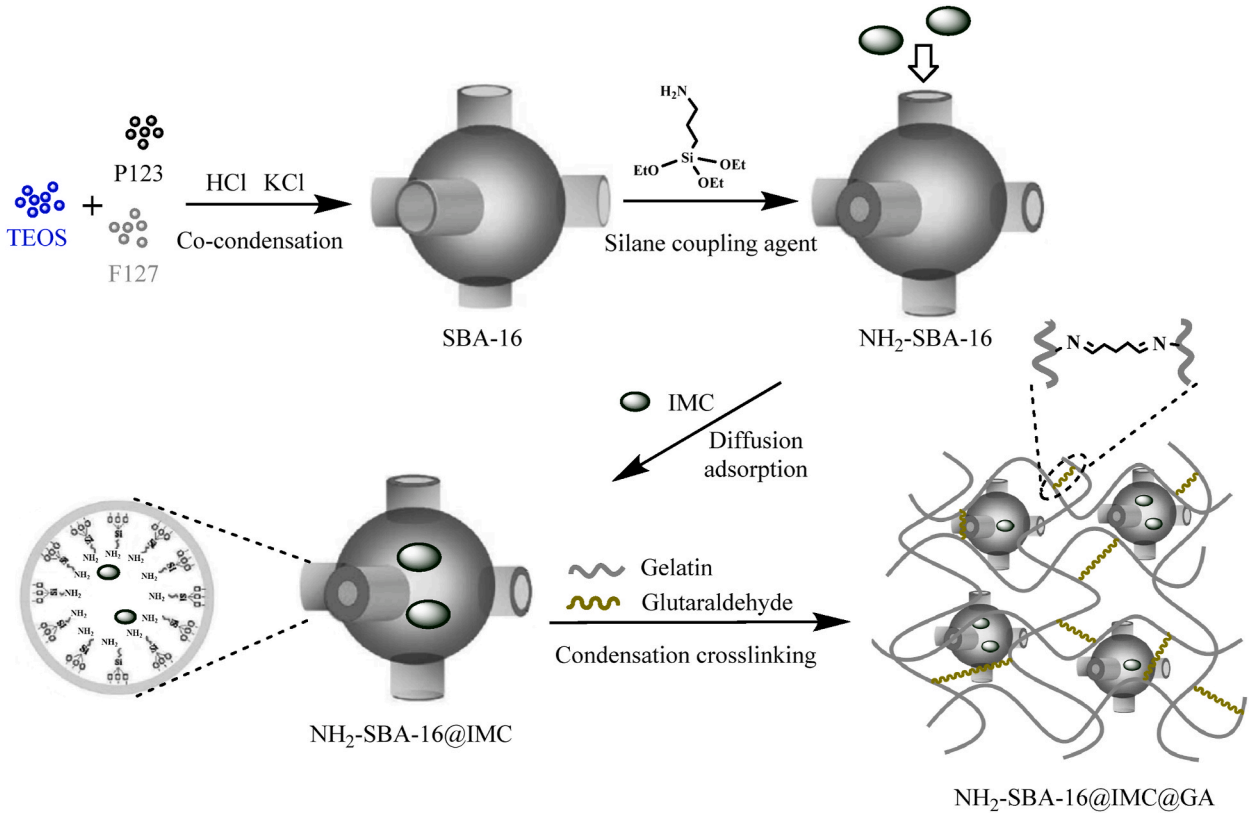

Scheme 1. Schematic representation of the preparation process of NH_2-SBA-16@IMC@GA drug-loaded composite.

glutaraldehyde (Scheme 1). The in vitro simulated release performance of the NH_2-SBA-16@IMC@GA was investigated under three pH conditions at 37 °C. The results showed that the drug-loaded composites were capable of responsive release in a specific pH environment and could effectively control the release rate of the drug IMC. According to the results, the release process of the drug-loaded composites NH_2-SBA-16@IMC@GA conformed to the first-order drug release equation and the Higuchi plane diffusion mode equation.

2. Experimental

2.1. Materials and chemicals

Tetraethyl orthosilicate (TEOS, 98%), 3-aminopropyl trimethoxysilane (APTMS, 99%), Pluronic P123 ($EO_{20}PO_{70}EO_{20}$), and Pluronic F127 ($EO_{106}PO_{70}EO_{106}$) were purchased from Sigma-Aldrich. Indometacin (IMC, 98%), Gelatin (GA, 98%), Glutaraldehyde (98%), Hydrochloric acid (HCl, 37%), Toluene (99%), Acetone (98%), Methanol (98%), and Potassium chloride (KCl, 98%) were purchased from Tianjin Chemical Plant. All chemical materials were used without further purification. Deionized water was used in all experiments.

2.2. Materials characterization

The FT-IR spectra were collected on a Thermofisher Nicolet-IS50 Fourier-Transform Infrared Spectrometer using a KBr pellet technique in the 4000–400 cm^{-1} range. The small-angle and wide-angle X-ray diffraction (XRD) patterns were obtained on a Rigaku Smartlab X-ray diffractometer keeping Cu Kα ($\lambda = 0.154$ nm) radiation at 45 kV and 30 mA. The scan 2θ range of small-angle XRD was set between 0.6° and 5° with a scan rate of 2° min^{-1} and 2θ between 10° and 70° with 10° min^{-1} for wide-angle measurements. Specific surface area, porosity, and pore volume of samples were evaluated on a Micromeritics model ASAP-2020 M instrument using the BET and BJH methods. The materials morphology was examined using an S-700 scanning electron microscopy (SEM) operating. TEM images were obtained on a JEOL JEM-2010 transmission electron microscope.

2.3. Preparation of drug-loaded composites

SBA-16 and NH_2-SBA-16 were prepared using a modified method from the literature [37,38]. A schematic diagram of the preparation of the NH_2-SBA-16@IMC@GA drug-loaded composite was shown in Scheme 1.

2.3.1. Preparation of SBA-16

Added 3 g of potassium chloride to 40 mL of hydrochloric acid solution at 35 °C, and then added 0.14 g P123 and 0.74 g F127 and stirred until it was completely dissolved [37]. Then 4.5 mL of TEOS was added, and stirring was continued for 24 h at room temperature. All the obtained mixed liquid was transferred to a polytetrafluoroethylene crystallization kettle, crystallized at 100 °C for 24 h, the obtained solid was washed and centrifuged, and dried at 45 °C in a vacuum for 48 h. Finally, the dried sample was placed in a tube furnace and calcined at 550 °C under air conditions for 6 h to remove the templating agent, and a white powdery solid SBA-16 was obtained.

2.3.2. Preparation of NH_2-SBA-16

Added dry 0.5 g of SBA-16 carrier to 25 mL of toluene at room temperature, and ultrasonically disperse for 45 min. Then 0.5 mL of APTMS was added, and the mixture was heated under reflux and stirred for 24 h under a nitrogen atmosphere [38]. The obtained solid was filtered and washed, and dried under vacuum at 80 °C for 24 h to obtain white powder NH_2-SBA-16 composite.

2.3.3. Preparation of SBA-16@IMC and NH_2-SBA-16@IMC drug-loaded precursors

The composite material is prepared by the adsorption equilibrium solvent evaporation method. Dissolve 0.5 g of indomethacin IMC in 25 mL acetone, add 1.0 g of NH_2-SBA-16 and sonicate for 1 h, then stir and adsorb at 37 °C for 24 h. The mixed system was vacuum dried at 55 °C, the solvent was slowly evaporated, milled, and washed, and the white solid was finally obtained as NH_2-SBA-16@IMC drug-loaded precursor. SBA-16@IMC drug-loaded precursor material was prepared via the same method but using SBA-16 instead of NH_2-SBA-16.

2.3.4. Preparation of SBA-16@IMC@GA and NH_2-SBA-16@IMC@GA drug-loaded composites

A 50 mg/mL gelatin solution was prepared at 40 °C, and then 1.0 g NH_2-SBA-16@IMC was uniformly dispersed in 20 mL of the prepared gelatin solution. The mixture was shaken in a shaker at 50 °C for 6 h, and then the deionized water was added at 4 °C, mixed evenly, and washed twice by centrifugation. Then slowly add 0.6 mL of 50% glutaraldehyde solution and stir for 2 h. Next, the samples were washed several times with deionized water and dried in a vacuum. Finally, a reddish-brown solid product was obtained, which was labeled as NH_2-SBA-16@IMC@GA (GA is expressed as the condensation polymer of gelatin with glutaraldehyde). SBA-16@IMC@GA drug-loaded composite was prepared via the same method but using SBA-16@IMC instead of NH_2-SBA-16@IMC.

3. Results and discussion

3.1. FT-IR spectra

The FT-IR spectra of IMC, SBA-16, NH_2-SBA-16, SBA-16@IMC, NH_2-SBA-16@IMC, SBA-16@IMC@GA, and NH_2-SBA-16@IMC@GA composites were presented in Fig. 1. It can be seen from the results that indomethacin IMC had a strong absorption peak near 1700 cm^{-1}, which was attributed to the carbonyl stretching vibration peaks in the amide and carboxyl groups in the structure; and the three absorption peaks at 1456, 1479, and 1590 cm^{-1} belonged to the skeleton vibration of the benzene ring, the above results proved that indomethacin was a carboxylic acid drug [39]. The carrier SBA-16 showed the characteristic absorption peak of a typical Si-O-Si bond at 1100 cm^{-1}. In the NH_2-SBA-16 material, a pair of weak absorption peaks at 2983 and 2937 cm^{-1} was attributed to the symmetric and asymmetric stretching vibrations of the saturated C–H bond. These results indicated that the aminopropyl group successfully modified to the surface of the carrier SBA-16. For the NH_2-SBA-16@IMC and SBA-16@IMC materials, the characteristic peaks of the aminopropyl group, Si-O-Si bond, and carboxylic acid appeared respectively, indicating that IMC had been encapsulated successfully in the NH_2-SBA-16 and SBA-16. For the gelatin-coated NH_2-SBA-16@IMC@GA and SBA-16@IMC@GA drug-loaded mesoporous materials, the C=O stretching vibration peak around 1719 cm^{-1} for IMC was significantly weakened. However, the absorption peak at 1688 cm^{-1} was significantly enhanced, which was attributed to the formation of imine bonds after the condensation of gelatin with glutaraldehyde, indicating that the drug-loaded porous materials were successfully encased in a layer of gelatin. Moreover, the characteristic absorption peaks of the benzene ring between 1450 and 1600 cm^{-1} of the two types of drug-loaded mesoporous materials were weakened, which also proved that the gelatin successfully encapsulated the drug-loaded carrier.

3.2. Small-angle XRD

The Fig. 2 were IMC, SBA-16, NH_2-SBA-16, SBA-16@IMC, NH_2-SBA-16@IMC, SBA-16@IMC@GA, and NH_2-SBA-16@IMC@GA composites of small-angle X-ray powder diffraction. According to the results, it can be seen that the drug IMC had no characteristic diffraction peaks and no ordered structure. The results showed that the carrier SBA-16 exhibited a strong diffraction peak at 0.81°, which belonged to the crystal plane diffraction peak of the (110) diffraction plane of the Im3m symmetric structure [37]. For the NH_2-SBA-16, SBA-16@IMC, and NH_2-SBA-16@IMC composites, their d_{100} crystal plane diffraction peaks still existed, but the peak intensity gradually decreased. Compared with the data of the SBA-16 carrier, the peak intensity of the d_{100} diffraction crystal plane in the NH_2-SBA-16@IMC composite sample with aminopropyl surface modifications and drug-coated IMC decreased, which can be explained by a large number of aminopropyl and the drug IMC structural unit entered the mesoporous channel in the NH_2-SBA-16@IMC, and the filling of the channel reduced the scattering contrast between the channel and the wall of the mesoporous material. For the two drug-loaded mesoporous materials SBA-16@IMC@GA and NH_2-SBA-16@IMC@GA, the crystal plane diffraction peaks of the d_{100} diffraction crystal plane further decreased, proving that the gelatin was successfully cross-linked and uniformly and densely encapsulated in the SBA-16@IMC and NH_2-SBA-16@IMC drug-loaded precursor.

3.3. Wide-angle XRD

The wide-angle XRD patterns of IMC, SBA-16, NH_2-SBA-16, SBA-16@IMC, NH_2-SBA-16@IMC, SBA-16@IMC@GA, and NH_2-SBA-16@IMC@GA materials were shown in Fig. 3. The results can be used to study the dispersion of drug IMC components in composites. A

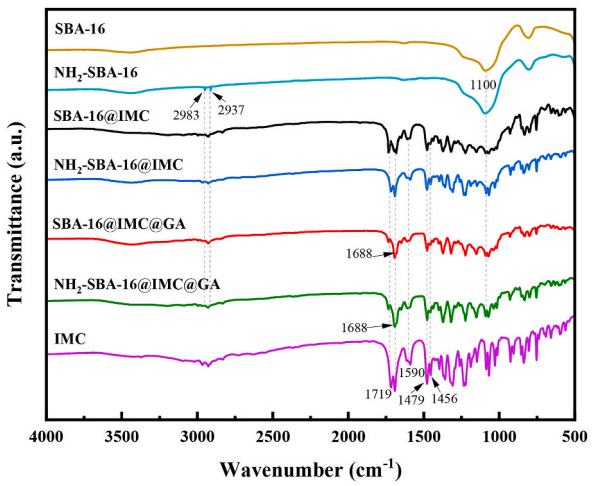

Fig. 1. The FT-IR spectra of IMC, SBA-16, NH_2-SBA-16, SBA-16@IMC, NH_2-SBA-16@IMC, SBA-16@IMC@GA and NH_2-SBA-16@IMC@GA composites.

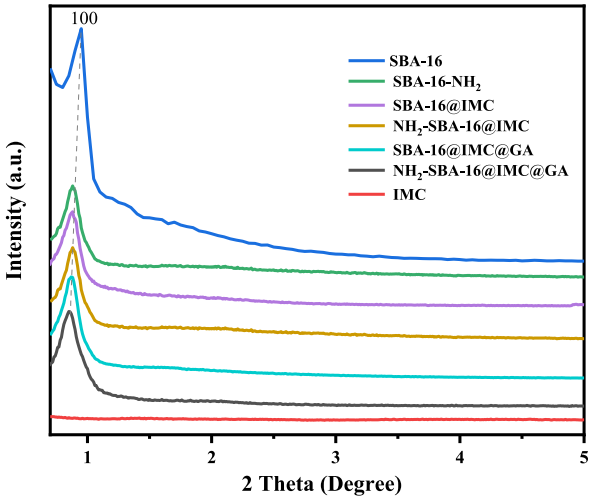

Fig. 2. The small-angle XRD patterns of IMC, SBA-16, NH_2-SBA-16, SBA-16@IMC, NH_2-SBA-16@IMC, SBA-16@IMC@GA and NH_2-SBA-16@IMC@GA.

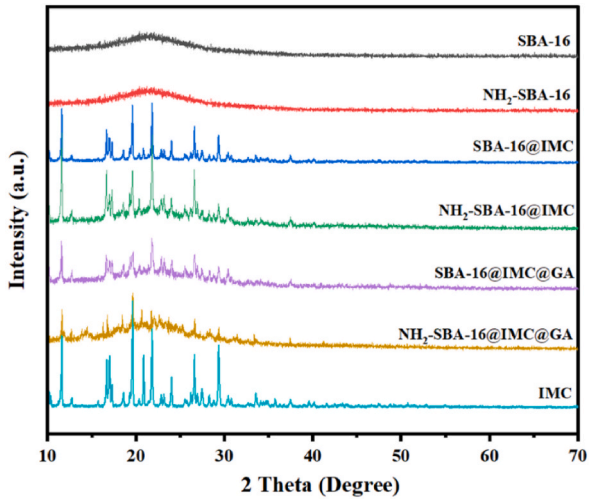

Fig. 3. The wide-angle XRD patterns of IMC, SBA-16, NH_2-SBA-16, SBA-16@IMC, NH_2-SBA-16@IMC, SBA-16@IMC@GA, and NH_2-SBA-16@IMC@GA.

broad diffraction peak ($2\theta = 15$-30°) was exhibited for the composite of carrier SBA-16 and aminopropyl-modified NH_2-SBA-16, which was a typical characteristic diffraction peak of amorphous silica. In the SBA-16@IMC and NH_2-SBA-16@IMC composites encapsulating the drug IMC components, the diffraction peaks of the drug IMC components appeared at 11.7°, 16.5°, 19.4°, 22.1°, and 26.7° respectively, in addition to the typical characteristic diffraction peaks of 15−30° amorphous silica. This indicates that the drug IMC was loaded on the mesoporous material on the mesoporous material without changing the crystal structure of the drug [40]. However, higher drug IMC loadings can cause them to disperse or aggregate unevenly in the composites. For the two drug-loaded mesoporous materials SBA-16@IMC@GA and NH_2-SBA-16@IMC@GA, when the composites were cross-linked with gelatin GA, the crystal plane diffraction peaks of the drug IMC components were significantly reduced, which proves that gelatin was successfully cross-linked and uniformly and densely wrapped around the SBA-16@IMC and NH_2-SBA-16@IMC mesoporous materials. Due to the introduction of gelatin polymer by the GA coating, the relative content of the IMC in the whole composite was subsequently reduced and its characteristic diffraction peaks were also reduced, and the above results were in agreement with the small-angle XRD.

3.4. N_2 adsorption-desorption analysis

It can be seen from the N_2 adsorption-desorption isotherm diagrams in Fig. 4 that the measured isotherms of SBA-16, NH_2-SBA-16, SBA-16@IMC, and NH_2-SBA-16@IMC samples belonged to the Type IV, and had a type H2 hysteresis ring. This type of isotherm was a major feature of nonionic surfactant-directed mesostructured materials. In the adsorption–desorption curves, the carrier SBA-16 was in

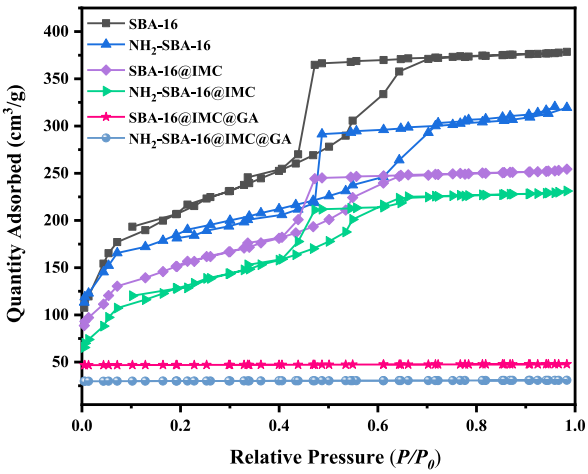

Fig. 4. The Nitrogen adsorption–desorption isotherms of IMC, SBA-16, NH_2-SBA-16, SBA-16@IMC, NH_2-SBA-16@IMC, SBA-16@IMC@GA, and NH_2-SBA-16@IMC@GA.

the range of $0.4 \leq P/P_0 \geq 0.7$, with a mesoporous sign of stagnation ring present, with the largest retention ring and pore volume among all tested materials. The hysteresis loop and pore volume of the aminopropyl-modified NH_2-SBA-16 material were lower than those of the carrier SBA-16. For the two composites SBA-16@IMC and NH_2-SBA-16@IMC coated with drug IMC, they still had retention rings marked by mesoporosity in this range. However, their retention rings and pores compared with the carrier SBA-16, the volume decreased significantly. For the two gelatin-coated drug-loaded composites SBA-16@IMC@GA and NH_2-SBA-16@IMC@GA, the test results showed that the BET specific surface area and pore size of the two drug-loaded materials were very small. The reason was that the cross-linking of GA and glutaraldehyde coats SBA-16@IMC and NH_2-SBA-16@IMC, which completely blocks the pores of the mesoporous material. This result demonstrated that gelatin successfully encapsulated SBA-16@IMC@GA and NH_2-SBA-16@IMC@GA materials.

3.5. Pore size distribution

BET specific surface area, pore size, and pore volume data of SBA-16, NH_2-SBA-16, SBA-16@IMC, NH_2-SBA-16@IMC, SBA-16@IMC@GA, and NH_2-SBA-16@IMC@GA composites were shown in Table 1. It can be seen from the pore size distribution diagrams in Fig. 5 that all materials had typical mesopore pore size distribution, and the narrow pore size distribution indicated that the composite materials prepared in this experiment had uniform pore channel distribution. It can be seen that the pore size distribution of the three materials NH_2-SBA-16, SBA-16@IMC, and NH_2-SBA-16@IMC gradually decreased. However, the test results for the drug-loaded mesoporous materials SBA-16@IMC@GA and NH_2-SBA-16@IMC@GA showed that the BET specific surface area, pore size, and pore volume of these two materials decreased sharply, the reason was caused by the complete blockage of the pores after gelatin and glutaraldehyde were condensed and cross-linked to coat the drug-loaded mesoporous material.

3.6. Thermal studies

The thermogravimetric curves of SBA-16, NH_2-SBA-16, SBA-16@IMC, NH_2-SBA-16@IMC, SBA-16@IMC@GA, and NH_2-SBA-16@IMC@GA materials were shown in Fig. 6. According to the results, the whole weight loss curve of the carrier SBA-16 was very stable, with a weight loss step at 70–150 °C, and the mass loss was 4.6%, which was caused by the volatilization of the water adsorbed on the surface of the silica. The residual amount of the NH_2-SBA-16 material was 85%. In addition to the adsorbed moisture, the weight loss step between 400 and 600 °C was the oxidative decomposition of the aminopropyl group functionalized on the surface of SiO_2. In the SBA-16@IMC and NH_2-SBA-16@IMC composites coated with drug IMC, relative to the carrier SBA-16 and NH_2-SBA-16, the weight loss step generated between 370 and 500 °C were the coating for the oxidative decomposition of the coated drug IMC, the masses of

Table 1
BET specific surface area, pore size, and pore volume data of composites.

Entry	Materials	$S_{BET}/m^2\ g^{-1}$	D_p/nm	$V_p/cm^3\ g^{-1}$
1	SBA-16	717	5.6	0.43
2	NH_2-SBA-16	494	4.8	0.34
3	SBA-16@IMC	236	4.7	0.17
4	NH_2-SBA-16@IMC	216	4.6	0.12
5	SBA-16@IMC@GA	18	–	0.01
6	NH_2-SBA-16@IMC@GA	14	–	0.01

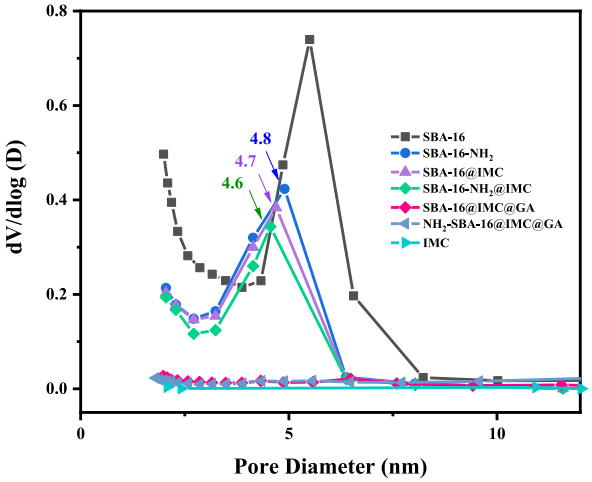

Fig. 5. The Pore size distribution of IMC, SBA-16, NH_2-SBA-16, SBA-16@IMC, NH_2-SBA-16@IMC, SBA-16@IMC@GA, and NH_2-SBA-16@IMC@GA.

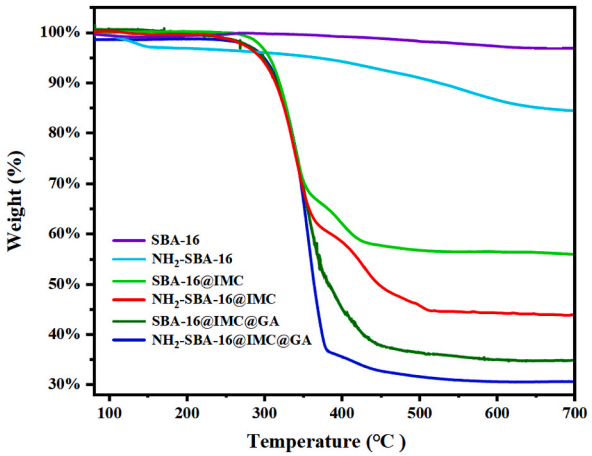

Fig. 6. The thermogravimetric curves of IMC, SBA-16, NH_2-SBA-16, SBA-16@IMC, NH_2-SBA-16@IMC, SBA-16@IMC@GA and NH_2-SBA-16@IMC@GA.

IMC were about 39.2 and 41.4% [41]. The residues of the drug-loaded composites SBA-16@IMC@GA and NH_2-SBA-16@IMC@GA were about 34% and 31%, and the weight loss step occurs between 370 and 500 °C, which were due to the oxidative decomposition of the coated drug, and the oxidative decomposition of the outer gelatin cross-linked film, the masses of gelatin film were about 22.2 and 29.4%. This result further proved that a dense gelatin cross-linked film was wrapped around the drug-carrying system.

3.7. TEM and SEM analyses

The electron microscope photos of SBA-16, NH_2-SBA-16, NH_2-SBA-16@IMC, and NH_2-SBA-16@IMC@GA materials were shown in Fig. 7. From the TEM image (Fig. 7A), it can be clearly observed that the carrier SBA-16 had a three-dimensional cage-like mesoporous structure with uniform pore size distribution and large pore volume. It can be seen from Fig. 7B that the SEM image of the carrier SBA-16 was in the aggregated state of nanoparticles. For NH_2-SBA-16, despite the surface functionalization of the support with 3-aminopropyl trimethoxysilane, its highly ordered mesoporous structure was still observed over a wide area, they have a uniform cubic symmetric (Im3m) pore structure (Fig. 7C and D). For NH_2-SBA-16@IMC, we can see that still exists in a three-dimensional cage-like structure even if the drug was loaded on the mesoporous material. The introduced drug moieties slightly agglomerated on the SiO_2 surface to form fine particles and increased the contact area (Fig. 7E and F). During the release process, the larger the surface contact area, the easier it was to be released, which can increase the dissolution rate of the drug. Comparing the TEM images of NH_2-SBA-16@IMC@GA and NH_2-SBA-16@IMC, there was a shadow outside the structure of the mesoporous material, indicating that gelatin was wrapped in NH_2-SBA-16@IMC (Fig. 7G). The encapsulating gelatin layer of the mesoporous material was thicker, resulting in a blurred mesoporous structure in TEM images. The SEM of NH_2-SBA-16@IMC@GA drug-loaded composite can clearly find that a dense gelatin film shadow was formed on the surface of the drug-loaded carrier, and the SEM image was consistent with the analysis result of

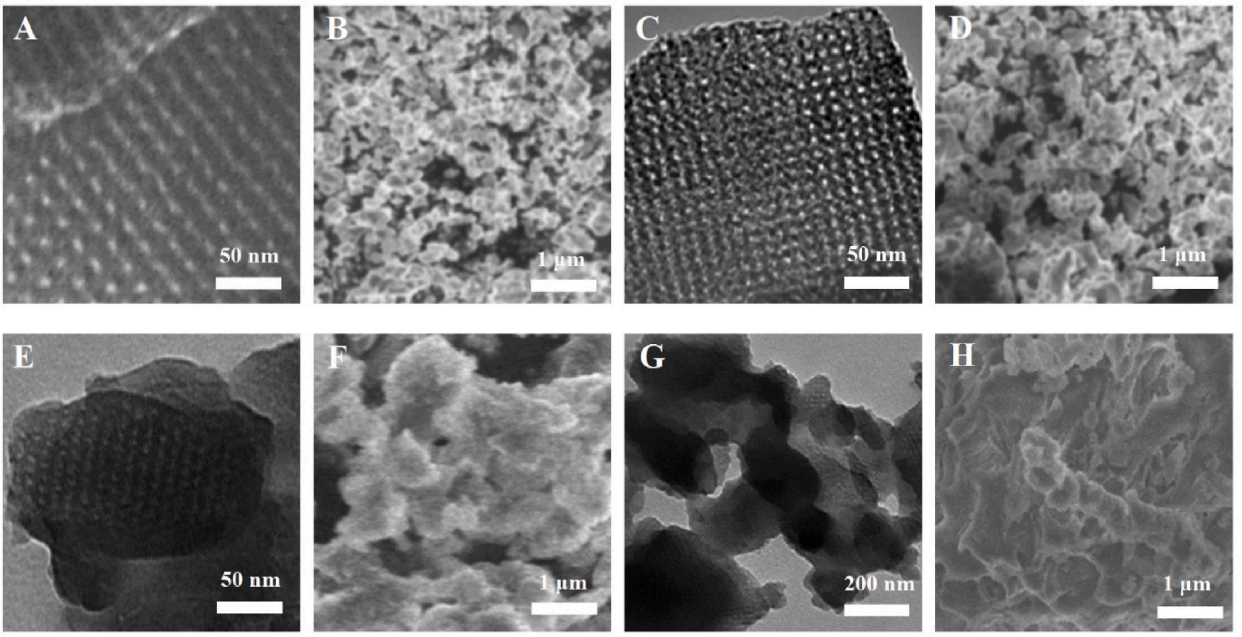

Fig. 7. The electron microscope photos of SBA-16 (A and B), NH_2-SBA-16 (C and D), NH_2-SBA-16@IMC (E and F), and NH_2-SBA-16@IMC@GA (G and H).

the TEM image (Fig. 7H).

3.8. *In vitro release studies*

The in vitro drug-released behavior of the composites under different pH conditions was studied by simulating the pH range of the gastrointestinal tract in vitro. Weighed 0.07 g of SBA-16@IMC, NH_2-SBA-16@IMC, SBA-16@IMC@GA, and NH_2-SBA-16@IMC@GA composites, respectively, and dispersed them into the shaped bottles containing 25 mL of phosphate buffer solution. Then placed in a constant temperature shaking shaker at 37 ± 1 °C for vigorous shaking in the dark. At regular intervals, 3 mL of the solution was taken out, and the absorbance of the drug in the solution was measured by a UV–Vis spectrophotometer. The drug IMC sustained-release properties of four drug-loaded materials (SBA-16@IMC, NH_2-SBA-16@IMC, SBA-16@IMC@GA, and NH_2-SBA-16@IMC@GA) was studied under three different conditions (pH values were 2.0, 6.8, and 7.4, respectively), and the cumulative release percentage was plotted as a function of time [42–44].

First, the drug release properties of the four drug-loaded composite materials were investigated under the strong acid condition of pH = 2.0, and the cumulative release rate curves were shown in Fig. 8. As can be seen from the curves, the two drug-loaded precursors,

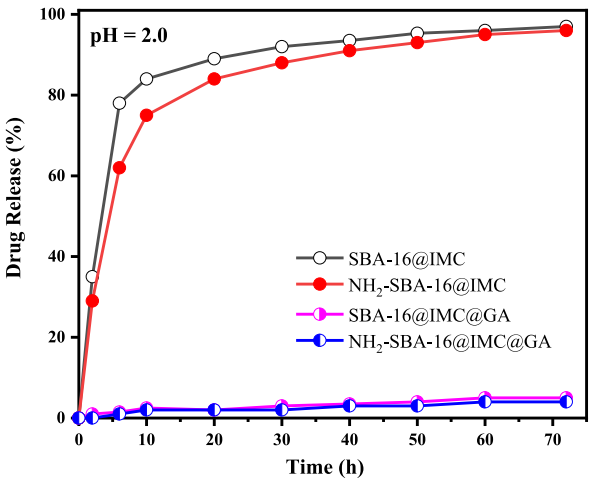

Fig. 8. Cumulative release of SBA-16@IMC, NH_2-SBA-16@IMC, SBA-16@IMC@GA, and NH_2-SBA-16@IMC@GA at pH = 2.0.

SBA-16@IMC and NH_2-SBA-16@IMC, without gelatin cross-linking coating, had a rapid release process for IMC in pH = 2.0 medium, reaching 62% and 78%, respectively, at 6 h. The slow release gradually leveled off after 24 h and reached more than 90% at 48 h. The final slow release was at about 95% level. This indicates that the drug IMC is directly desorbed from the pores and surfaces of the composite in an acid solution. For the two drug-loaded materials, SBA-16@IMC@GA and NH_2-SBA-16@IMC@GA, which were coated with gelatin cross-linking, basically no drug release occurred under these conditions. It was shown that the two drug-loaded materials SBA-16@IMC@GA and NH_2-SBA-16@IMC@GA had no sustained drug release properties under strong acid conditions, because the gelatin polymer did not swell under strong acid conditions.

According to Fig. 9, in the phosphate buffer solution of pH = 7.4, the SBA-16@IMC and NH_2-SBA-16@IMC drug-loaded precursors that were not encapsulated by gelatin both released significantly at 6 h and the release rate reached more than 60% (reached 63% and 78%, respectively). This result was similar to the release curve at pH = 2.0, indicating that the drug released of SBA-16@IMC and NH_2-SBA-16@IMC drug-loaded precursors was not affected by the environment and did not show a response to pH value. In the treatment of colon diseases, it was generally required that the drug release starts at 6 h. From the results in Fig. 9, it can be seen that the drug release of the two drug-loaded precursors SBA-16@IMC and NH_2-SBA-16@IMC did not reach 6 h. It had been released in large quantities and will affect the effect of the drug. For the gelatin-coated SBA-16@IMC@GA and NH_2-SBA-16@IMC@GA drug-loaded composites, the drug IMC release amounts were only 35% and 21% at 6 h, respectively, and sustained drug release in the subsequent period, The total drug release after 72 h was 85% and 86%. After comparing the curves in the figure, under the condition of pH = 7.4, the two drug-loaded composites of SBA-16@IMC@GA and NH_2-SBA-16@IMC@GA coated with gelatin released the drug, showing that the pH conditions responsiveness. Moreover, compared with the SBA-16@IMC@GA composites, the aminopropyl-modified NH_2-SBA-16@IMC@GA drug-loaded material had a higher drug release rate and a longer duration. The reason was that the aminopropyl group in the carrier had an acid-base effect with the carboxylic acid IMC drug, which increased the drug loading of the composite material, and the release of the IMC drug continues under the action of the aminopropyl group.

According to the drug-released results in Figs. 8 and 9, it had been concluded that under the condition of pH = 2.0, the two materials SBA-16@IMC and NH_2-SBA-16@IMC had no acid-base responsiveness. At pH = 7.4, although the two composites SBA-16@IMC@GA and NH_2-SBA-16@IMC@GA exhibited pH responsiveness, the 3-aminopropyl-modified NH_2-SBA-16@IMC@GA compared with SBA-16@IMC@GA composites, SBA-16@IMC@GA had a higher rate of drug release and longer duration. Therefore, we chose the NH_2-SBA-16@IMC@GA composite to simulate the pH value of the gastrointestinal tract in vitro, and investigated its drug IMC sustained release properties under three different conditions (pH values were 2.0, 6.8, 7.4, respectively). It can be seen from Fig. 10 that under the strong acid condition of pH = 2.0, the NH_2-SBA-16@IMC@GA composite did not release the drug. Under the weak acidity of pH = 6.8, the gelatin swelled, and the drug IMC began to be released from the NH_2-SBA-16@IMC@GA composite. The release amount was 12% at 6 h and then tended to be constant. After 72 h, the total release amount was only 41%. The gelatin swelled significantly under the weak alkaline pH = 7.4, the release rate of drug IMC in the NH_2-SBA-16@IMC@GA composite material was significantly accelerated, and the release amount reached 21% at 6 h, and the total release amount reached 86% after 72 h. The above results showed that the NH_2-SBA-16@IMC@GA composites coated with gelatin did not release the drug in a strong acid environment; they release slowly under weak acid conditions, while under weak alkaline conditions, the drug release rate was significantly increased. Therefore, within a certain pH range, the gelatin-coated NH_2-SBA-16@IMC@GA mesoporous drug-loaded composite had a pH-responsive effect (Scheme 2).

The release mechanism is an important part of the study of sustained and controlled release formulations, and we usually use the kinetic equation as the method to study the release mechanism [45, 46, 47]. The kinetic equation is a commonly used drug release kinetic equation based on Fick's diffusion rule and some boundary conditions and assumptions. The model equations are zero-order kinetic equation, Hixson-Crowell dissolution equation, first-order kinetic equation, and Higuchi plane diffusion kinetic equation (Table 2).

where Q is the cumulative release percentage, t is the sampling time, and k is a constant. The release data of NH_2-SBA-16@IMC@GA drug-loaded mesoporous composites were fitted, and the results are shown in Table 2.

The zero-order kinetic equation, Hixson-Crowell dissolution equation, first-order kinetic equation, and Higuchi plane diffusion kinetic equation were used to model the release data of the drug-loaded mesoporous material in vitro at pH = 7.4. According to the results, the release process of the drug-loaded mesoporous material NH_2-SBA-16@IMC@GA conformed to the first-order drug release equation and the Higuchi plane diffusion mode equation. Therefore, the release process of the drug-loaded mesoporous material NH_2-SBA-16@IMC@GA was in line with the release characteristics of sustained-release preparations, and also in line with the drug release rules.

4. Conclusion

In this paper, a pH-responsive gelatin-encapsulated amino-modified drug-loaded porous composite was prepared by post-synthesis-encapsulation technology. Through various characterization techniques, it was proved that in the NH_2-SBA-16@IMC@GA drug-loaded mesoporous composite, the drug IMC was adsorbed by the mesoporous material and its structure was retained, and the gelatin was successfully cross-linked and uniformly and densely encapsulated around the NH_2-SBA-16@IMC material. Under 37 ± 1 °C, the different media (pH is 2.0, 6.8, and 7.4, respectively), in vitro simulation release properties of drug composites. The results show that the drug composite material can be released in response to the pH environment, which can effectively control the release speed of the drug indomethacin. During the in vitro release study, the release amounts of the NH_2-SBA-16@IMC@GA composite under three different pH environments were 5%, 41%, and 86%, respectively, proving that it has certain pH responsiveness. When the pH = 7.4, the drug release of NH_2-SBA-16@IMC@GA was 21.0% at 6 h and could reach 86% at 72 h. Composites had a high drug load and long

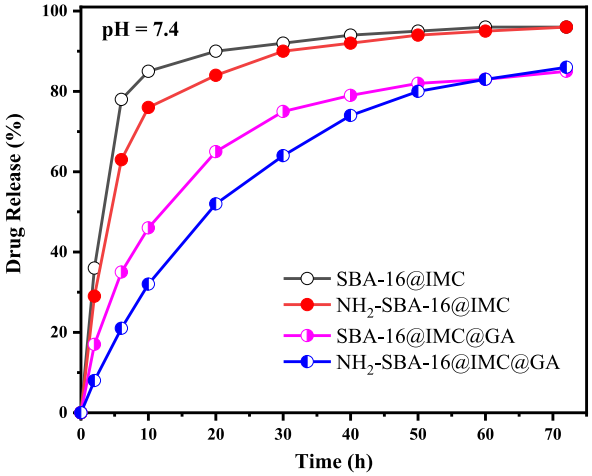

Fig. 9. Cumulative release of SBA-16@IMC, NH_2-SBA-16@IMC, SBA-16@IMC@GA, and NH_2-SBA-16@IMC@GA at pH = 7.4.

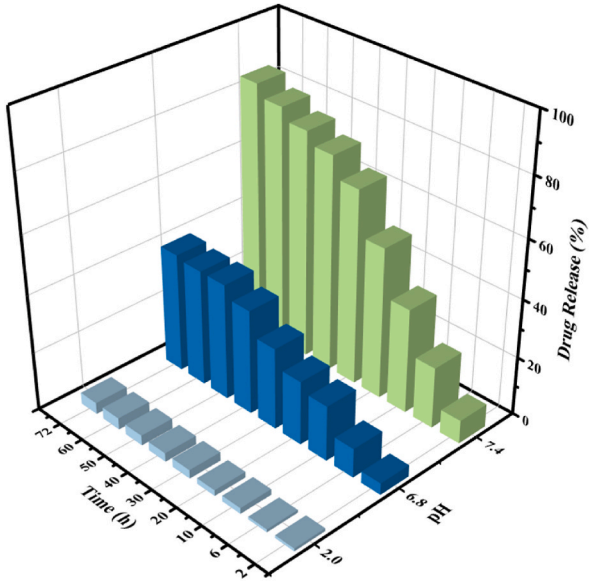

Fig. 10. Drug release of NH_2-SBA-16@IMC@GA under different pH conditions.

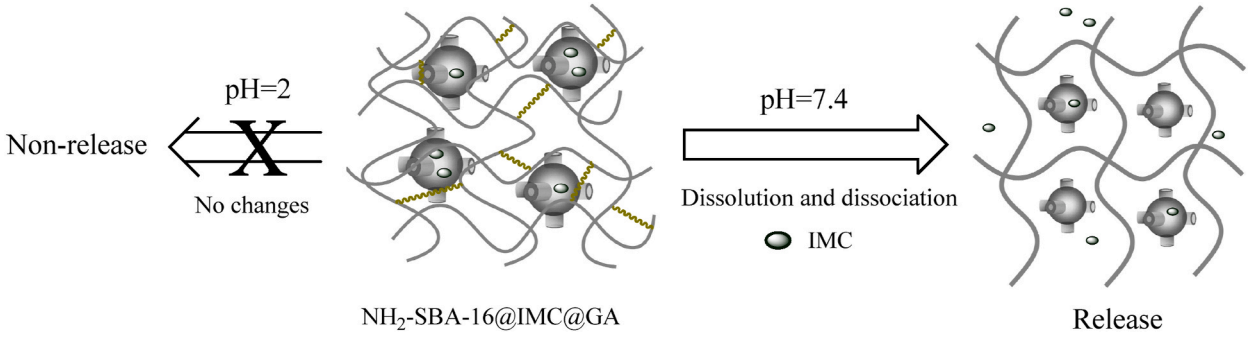

Scheme 2. Schematic diagram of the pH-responsive slow release of the NH_2-SBA-16@IMC@GA drug-loaded composite.

Table 2
Model and Fitting Equation of NH_2-SBA-16@IMC@GA drug-loaded material.

Entry	Kinetic equation	Model Equation	Fitting Equation	R^2
1	Zero-order kinetic equation	$Q = Kt$	$Q = 0.47131t-55.8$	0.7979
2	Hixson-Crowell erosion equation	$(100 - Q)^{1/3} = -Kt$	$(100-Q)^{1/3} = 3.55077 + 0.01654t$	0.9022
3	First-order kinetic equation	$\ln(100 - Q) = -Kt$	$\ln(100-Q) = 3.81369–0.01634t$	0.91715
4	Higuchi plane diffusion kinetic equation	$Q = Kt^{1/2}$	$Q = 5.06808t^{1/2}+44.65708$	0.91999

sustained release time. It showed that the mesoporous material can effectively carry the medicine, stable and slow release, in the smooth and continuous drug release in the simulated environment. According to the results, the release process of the drug-loaded mesoporous material NH_2-SBA-16@IMC@GA conformed to the first-order drug release equation and the Higuchi plane diffusion mode equation. Therefore, the release process of the drug-loaded mesoporous material NH_2-SBA-16@IMC@GA was in line with the release characteristics of sustained-release preparations, and also in line with the drug release rules.

Declarations

Author contribution statement

Jianglei Hu: Conceived and designed the experiments; Wrote the paper; Analyzed and interpreted the data. Fengwei Shi: Conceived and designed the experiments; Wrote the paper; Contributed reagents, materials, analysis tools or data. Bo Yu, Ruiping Shi: Performed the experiments; Analyzed and interpreted the data; Zelong Liu, Peihang Shen: Performed the experiments; Chunlai Liu: Analyzed and interpreted the data; Contributed reagents, materials, analysis tools or data. Materials-methods.

Funding statement

Mr. Jianglei Hu was supported by Project for Science & Technology Development of Jilin Province, China [20220101095JC].

Data availability statement

Data will be made available on request.

Declaration of interest's statement

The authors declare no competing interests.

References

[1] T. Jones, N. Saba, Nanotechnology and drug delivery: an update in oncology, Pharmaceutics 3 (2011) 171–185.
[2] M. Irshad, N. Iqbal, A. Mujahid, A. Afzal, T. Hussain, A. Sharif, E. Ahmad, M. Athar, Molecularly imprinted nanomaterials for sensor applications, Nanomaterials 3 (2013) 615–637.
[3] M. Eaton, Nanomedicine: industry-wise research, Nat. Mater. 6 (2007) 251–253.
[4] C. Schmidt, J. Storsberg, Nanomaterials-tools, technology and methodology of nanotechnology based biomedical systems for diagnostics and therapy, Biomedicines 3 (2015) 203–223.
[5] W. Huang, G. Xiao, Y.J. Zhang, W.P. Min, Research progress and application opportunities of nanoparticle–protein corona complexes, Biomed. Pharmacother. 139 (2021) 111541–111546.
[6] S.A. Sun, Q. Han, S.Y. Tan, Y. Long, Q.L. Liang, M.Y. Ding, A magnetic, luminescent and mesoporous nanocomposite as protein drug Carrier, Microporous Mesoporous Mater. 277 (2019) 261–266.
[7] D. Walczyk, F.B. Bombelli, M.P. Monopoli, I. Lynch, K.A. Dawson, What the cell "Sees" in bionanoscience, J. Am. Chem. Soc. 132 (2010) 5761–5768.
[8] S.R. Saptarshi, A. Duschl, A. Lopata, Interaction of nanoparticles with proteins: relation to bio-reactivity of the nanoparticle, J. Nanobiotechnol. 11:26 (2013) 1–12.
[9] W. Poon, B.R. Kingston, B. Ouyang, W. Ngo, W.C.W. Chan, A framework for designing delivery systems, Nat. Nanotechnol. 15 (2020) 819–829.
[10] Z. Ban, P. Yuan, F. Yu, T. Peng, Q. Zhou, X. Hu, Machine learning predicts the functional composition of the protein corona and the cellular recognition of nanoparticles, Proc. Natl. Acad. Sci. U. S. A. 117 (2020) 10492–10499.
[11] C.T. Kresge, M.E. Leonowicz, W.J. Roth, J.C. Vartuli, J.S. Beck, Ordered mesoporous molecular sieves synthesized by a liquid-crystal template mechanism, Nature 359 (1992) 710–712.
[12] M. Vallet-Regi, A. Rámila, R.P. del Real, J. Pérez-Pariente, A new property of MCM-41: drug delivery system, Chem. Mater. 13 (2001) 308–311.
[13] V. Ambrogi, L. Perioli, F. Marmottini, S. Giovagnoli, M. Esposito, C. Rossi, Improvement of dissolution rate of piroxicam by inclusion into MCM-41 mesoporous silicate, Eur. J. Pharmaceut. Sci. 32 (2007) 216–222.
[14] T. Heikkila, J. Salonen, J. Tuura, M.S. Hamdy, G. Mul, N. Kumar, T. Salmi, D.Y. Murzin, L. Laitinen, A.M. Kaukonen, J. Hirvonen, V.P. Lehto, Mesoporous silica material TUD-1 as a drug delivery system, Int. J. Pharm. 331 (2007) 133–138.
[15] M. Manzano, V. Aina, C.O. Areán, F. Balas, V. Cauda, M. Colilla, M.R. Delgado, M. Vallet-Regí, Studies on MCM-41 mesoporous silica for drug delivery: effect of particle morphology and amine functionalization, Chem. Eng. J. 137 (2008) 30–37.
[16] Q. Tang, Y. Xu, D. Wu, Y. Sun, J. Wang, J. Xu, F. Deng, Studies on a new carrier of trimethylsilyl-modified mesoporous material for controlled drug delivery, J. Contr. Release 114 (2006) 41–46.
[17] A. Szegedi, M. Popova, I. Goshev, S. Klébert, J. Mihály, Controlled drug release on amine functionalized spherical MCM-41, J. Solid State Chem. 194 (2012) 257–263.

[18] Q.L. Tang, Y. Xu, D. Wu, Y.H. Sun, J.Q. Wang, J. Xu, F. Deng, Studies on a new carrier of trimethylsilyl-modified mesoporous material for controlled drug delivery, J. Contr. Release 114 (2006) 41–46.
[19] E. Abe, S.J. Pennycook, A.P. Tsai, Direct observation of a local thermal vibration anomaly in a quasicrystal, Nature 421 (2003) 347–350.
[20] N.K. Mal, M. Fujiwara, Y. Tanaka, T. Taguchi, M. Matsukata, Photo-switched storage and release of guest molecules in the pore void of coumarin-modified MCM-41, Chem. Mater. 15 (2003) 3385–3394.
[21] W. Zhao, J. Gu, L. Zhang, H. Chen, J. Shi, Fabrication of uniform magnetic nanocomposite spheres with a magnetic core-mesoporous silica shell structure-support, J. Am. Chem. Soc. 127 (2005) 8916–8917.
[22] L. Han, C. Tang, C. Yin, Dual-targeting and pH/redox-responsive multi-layered nanocomplexes for smart co-delivery of doxorubicin and siRNA, Biomaterials 60 (2015) 42–52.
[23] Y. Zhu, J. Shi, W. Shen, X. Dong, J. Feng, M. Ruan, Y. Li, Stimuli-responsive controlled drug release from a hollow mesoporous silica sphere/polyelectrolyte multilayer core-shell structure, Angew. Chem. 117 (2005) 5213–5217.
[24] Y.F. Zhu, J.L. Shi, A mesoporous core-shell structure for pH-controlled storage and release of water-soluble drug, Microporous Mesoporous Mater. 103 (2007) 243–249.
[25] Y.H. Cui, R. Deng, X.S. Li, X.H. Wang, Q. Jia, E. Bertrand, K. Meguellati, Y.-W. Yang, Temperature-sensitive polypeptide brushes-coated mesoporous silica nanoparticles for dual-responsive drug release, Chin. Chem. Lett. 30 (2019) 2291–2294.
[26] M.T.A. Samri, A.V. Birader, A.R. Alsuwaidi, G. Balhaj, S. Al-Hammadi, S. Shehab, S. Al-Salam, S. Tariq, T. Pramathan, S. Benedict, T. Asefa, A.K. Souid, In vitro biocompatibility of calcined mesoporous silica particles and fetal blood cells, Int. J. Nanomed. 7 (2012) 3111–3121.
[27] C. Cara, E. Rombi, A. Musinu, V. Mameli, A. Ardu, M.S. Angotzi, L. Atzori, D. Niznansky, H.L. Xin, C. Cannas, MCM-41 support for ultrasmall γ-Fe_2O_3 nanoparticles for H_2S removal, J. Mater. Chem. 5 (2017) 21688–21698.
[28] S. Rubino, M.L. Saladino, R. Busà, D.F.C. Martino, M.A. Girasolo, E. Caponetti, L. Tesoriere, A. Attanzio, Loading and release of the complex [Pt(DTBTA)(DMSO)Cl]Cl•$CHCl_3$ with the 2,2′-dithiobis(benzothiazole) ligand into mesoporous silica and studies of antiproliferative activity on MCF-7 cells, Polyhedron 153 (2018) 234–239.
[29] S.T. Song, X.F. Zhou, A.J. Duan, Z. Zhao, K.B. Chi, M.H. Zhang, G.Y. Jiang, J. Liu, J.M. Li, X.L. Wang, Synthesis of mesoporous silica material with ultra-large pore sizes and the HDS performance of dibenzothiophene, Microporous Mesoporous Mater. 226 (2016) 510–521.
[30] C. Vanichvattanadecha, W. Singhapong, A. Jaroenworaluck, Different sources of silicon precursors influencing on surface characteristics and pore morphologies of mesoporous silica nanoparticles, Appl. Surf. Sci. 513 (2020) 145568–145582.
[31] R.S. Gudiña, S.Y. Vilar, M.G. Gómez, Z.V. Osorio, M.D.L. Fuente, Y.P. Redondo, R. López, J. Rivas, Versatile mesoporous nanoparticles for cell applications, J. Nanosci. Nanotechnol. 21 (2021) 2824–2833.
[32] I. Trendafilova, Á. Szegedi, K. Yoncheva, P. Shestakova, J. Mihály, A. Ristić, S. Konstantinov, M. Popova, A pH dependent delivery of mesalazine from polymer coated and drug-loaded SBA-16 systems, Eur. J. Pharmaceut. Sci. 81 (2016) 75–81.
[33] M. Maraldi, M. Lisi, G. Moretti, M. Sponchioni, D. Moscatelli, Health care-associated infections: controlled delivery of cationic antiseptics from polymeric excipients, Int. J. Pharm. 607 (2021) 120956–120969.
[34] I. Trendafilova, H. Lazarova, R. Chimshirova, B. Trusheva, N. Koseva, M. Popova, Novel kaempferol delivery systems based on Mg-containing MCM-41 mesoporous silicas, J. Solid State Chem. 301 (2021) 122323–122332.
[35] R.J. Patel, A.A. Patel, H.P. Patel, Stabilized amorphous state of riluzole by immersion-rotavapor method with synthesized mesoporous SBA-15 carrier to augment in-vitro dissolution, J. Drug Deliv. Sci. Technol. 61 (2021) 102270–102293.
[36] M.V. Dumitru, T. Sandu, A.L. Ciurlică, I.E. Neblea, B. Trică, A. Ghebaur, S.A. Gârea, H. Iovu, A. Sârbu, T.V. Iordache, Organically modified montmorillonite as pH versatile carriers for delivery of 5-aminosalicylic acid, Appl. Clay Sci. 218 (2022) 106415–106424.
[37] J.L. Hu, Q.Y. Wu, W. Li, L. Ma, F. Su, Y.H. Guo, Y.Q. Qiu, Epoxidation of alkenes catalyzed by phenyl group-modified, periodic mesoporous organosilica-entrapped, dimeric manganese–salen complexes, ChemSusChem 4 (2011) 1813–1822.
[38] J.L. Hu, K.X. Li, W. Li, F.Y. Ma, Y.H. Guo, Selective oxidation of styrene to benzaldehyde catalyzed by Schiff base-modified ordered mesoporous silica materials impregnated with the transition metal-monosubstituted Keggin-type polyoxometalates, Appl. Catal. Gen. 364 (2009) 211–220.
[39] N. Yuksel, M. Baykara, H. Shirinzade, S. Suzen, Investigation of triacetin effect on indomethacin release from poly (methyl methacrylate) microspheres: evaluation of interactions using FT-IR and NMR spectroscopies, Int. J. Pharm. 404 (2011) 102–109.
[40] C.J. Benmore, S.R. Benmore, A.D. Edwards, C.D. Shrader, M.H. Bhat, B.R. Cherry, P. Smith, F. Gozzo, C. Shi, D. Smith, J.L. Yarger, S.R. Byrn, J.K.R. Weber, A high energy X-ray diffraction study of amorphous indomethacin, J. Pharmacol. Sci. 111 (2022) 818–824.
[41] V. Zeleňák, D. Halamová, M. Almáši, L. Žid, A. Zeleňáková, O. Kapusta, Ordered cubic nanoporous silica support MCM-48 for delivery of poorly soluble drug indomethacin, Appl. Surf. Sci. 443 (2018) 525–534.
[42] A. Froelich, T. Osmałek, A. Snela, P. Kunstman, B. Jadach, M. Olejniczak, G. Roszak, W. Białas, Novel microemulsion-based gels for topical delivery of indomethacin: formulation, physicochemical properties and in vitro drug release studies, J. Colloid Interface Sci. 507 (2017) 323–336.
[43] K. Kamburova, K. Mitarova, T. Radeva, Polysaccharide-based nanocapsules for controlled release of indomethacin, Colloid. Surface. 519 (2017) 199–204.
[44] Y.M. Han, J.M. Park, S. Her, M.S. Kim, Y.J. Park, K.B. Hahm, Revaprazan prevented indomethacin-induced intestinal damages by enhancing tight junction related mechanisms, Biochem. Pharmacol. 182 (2020) 114290–114305.
[45] B. Shekunov, E.R. Montgomery, Theoretical analysis of drug dissolution: I. Solubility and intrinsic dissolution rate, J. Pharmacol. Sci. 105 (2016) 2685–2697.
[46] K. Nagaraja, K.M. Rao, G.V. Reddy, K.S.V.K. Rao, Tragacanth gum-based multifunctional hydrogels and green synthesis of their silver nanocomposites for drug delivery and inactivation of multidrug resistant bacteria, Int. J. Biol. Macromol. 174 (2021) 502–511.
[47] Z.H. Li, M. Cai, K. Yang, P.L. Sun, Kinetic study of d-limonene release from finger citron essential oil loaded nanoemulsions during simulated digestion in vitro, J. Funct.Foods 58 (2019) 67–73.